

Fantastic Breaks: A Dataset of Paired 3D Scans of Real-World Broken Objects and Their Complete Counterparts

Nikolas Lamb, Benjamin Molloy, Cameron Palmer, Sean Banerjee, Natasha Kholgade Banerjee
Clarkson University, Potsdam NY, USA

{lambne, molloybr, campalme, sbanerje, nabernje}@clarkson.edu

Abstract

Automated shape repair approaches currently lack access to datasets that describe real-world damage geometry. We present Fantastic Breaks (and Where to Find Them: <https://terascale-all-sensing-research-studio.github.io/FantasticBreaks>), a dataset containing scanned, waterproofed, and cleaned 3D meshes for 78 broken objects, paired and geometrically aligned with complete counterparts. Fantastic Breaks contains class and material labels, synthetic proxies of repair parts that join to broken meshes to generate complete meshes, and manually annotated fracture boundaries. Through a detailed analysis of fracture geometry, we reveal differences between Fantastic Breaks and datasets of synthetically fractured objects generated using geometric and physics-based methods. We show experimental results of shape repair with Fantastic Breaks using multiple learning-based approaches pre-trained using a synthetic dataset and re-trained using a subset of Fantastic Breaks.

1. Introduction

Damage to objects is an expected occurrence of everyday real-world usage. However, when damage occurs, objects that could be repaired are often thrown out. Additive manufacturing techniques are rapidly becoming accessible at the consumer level, with 3D printing technologies available for materials such as plastics, metals, and even ceramics and wood. Though to date, practical approaches for repair have been largely manual and restricted to niche areas such as cultural heritage restoration, a large body of recent research has emerged on the automated reversal of damage, including reassembly using 3D scans of fractured parts [4, 9, 15, 17, 19–21, 34, 35, 46, 48, 49], or generation of new repair parts when portions of the original object are irretrievably lost due to damage [16, 18, 26–28, 30, 31, 36, 43, 44]. Geometry-driven approaches based on shape matching [4, 15, 16, 19–21, 25, 30, 31, 34–36, 43, 44], being

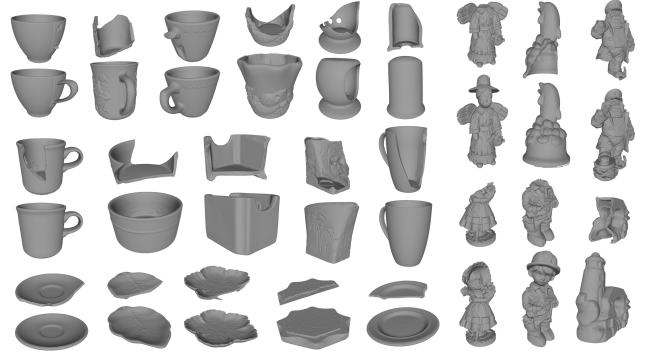


Figure 1. We present *Fantastic Breaks*, a dataset of 3D scans of real-world broken objects (top) aligned to 3D scans of complete counterparts (bottom). Objects span classes such as mugs, plates, figurines, jars, and bowls—household items prone to damage.

limited in their ability to be usable for objects of unknown complete geometry, have given way to learning-driven approaches [9, 17, 18, 26–28, 46, 48] aimed at generalization to repair at a large scale.

However, a principal challenge limiting understanding real-world damage and learning how to perform repair is that datasets of real-world damage for consumer space objects are virtually non-existent. Current learning-driven approaches for repair use datasets where fracture-based damage is synthetically generated using geometric approaches such as Boolean operations with primitives [9, 16, 26–29]. As they make assumptions about the fracture process rather than using data-driven fracture generation, such geometric methods are unlikely to be generalizable to real-world damage. Through *Breaking Bad*, Sellán et al. [41] have taken a first step toward large-scale fracture dataset generation. The *Breaking Bad* dataset consists of 3D shapes from Thingi10k [50] and PartNet [33] that have been subjected to physics-based damage using fracture modes [40]. By removing macro-scale shape assumptions embodied by geometric primitives, *Breaking Bad* is a promising step for research in shape assembly and repair. However, fractures

in Breaking Bad suffer from typical issues of resolution and simulation time step size that underlie physics simulations. The dataset is thus unfortunately hindered in providing a faithful representation of real-world damage.

In this work, we contribute *Fantastic Breaks*, the first dataset of 3D scans of damaged objects paired with 3D scans of their complete non-damaged counterparts, as shown in Figure 1. Each damaged object—hereafter referred to as a broken object due to the nature of damage suffered—is 3D scanned and geometrically registered to a 3D scan of the complete object prior to damage, such that intact regions of the complete and broken scans are aligned. Currently, the dataset contains 78 broken/complete pairs.

Our damage infliction often leaves one broken part intact, destroying or over-fragmenting the remainder of the object. We use an off-the-shelf subtraction-based approach [25] to synthetically generate repair part proxies from the intact broken part aligned to its complete counterpart. We also provide manually annotated class labels, material labels, and the fractured region on the broken mesh. Our work emulates the endeavor of groups in vision and robotics that contribute datasets of 3D scanned everyday-use objects [5, 6, 12, 23, 42]. Our analysis of real-world fracture properties of objects in *Fantastic Breaks* reveals fine-scale structure that enables *Fantastic Breaks* to overcome the drawbacks of synthetic datasets. We use our dataset to evaluate existing approaches to automatically generate new repair parts for broken shapes.

We summarize our contributions as follows:

1. We contribute the first 3D scanned real-world dataset of geometrically aligned broken/complete object pairs.
2. We provide class, material, and fracture surface annotations, and ground truth repair part proxies.
3. We contribute a geometric analysis of *Fantastic Breaks* in comparison to existing synthetic fracture datasets.
4. We provide evaluations of existing shape repair approaches using *Fantastic Breaks*.

2. Related Work

Fracture Datasets. Existing real-world fracture collections are restricted to scanning of multiple shards corresponding to a small set of originally intact objects, e.g., 7 objects [21], 3 frescoes [4], and 3 large-scale structures (Akrotiri settlement, Tongeren Roman excavation, and one fresco) [15]. Since fracture acquisition is performed post-damage for historical objects where no known counterparts exist, the datasets lack knowledge of the complete proxies. The Hampson Museum cultural heritage dataset [38] contains 3D scans for 138 cultural heritage objects. The dataset lacks paired damaged/complete data, or annotations to reveal what objects are damaged and what are intact, preventing them from being used to train repair or assembly approaches. Hong et al. [20] show assembly results using

a dataset of 5 shattered pots, with 3D scans acquired for the shattered fragments and the original pots. The original scans are used as evaluation oracles. Lamb et al. [25] repair 22 damaged objects by subtracting the damaged objects from *a priori* known complete proxies. Shell objects have their interiors filled prior to scanning.

Recognizing the need for large-scale datasets for learning-driven repair, a few datasets contain synthetic or scanned models subjected to synthetic fracture using geometric techniques such as subtracting primitives [9, 16, 26–29], or using physics models of fracture [41]. As we demonstrate in Section 4, real-world physical damage demonstrates geometric characteristics that differ from the break patterns of synthetically generated damage. Geometric fracture models [9, 16, 26–29] are only as precise as the primitive being used for fracture, e.g., Chen et al. [9] use five simplistic cut functions—planar, sine, parabolic, square, and pulse—modeled as oriented height fields. Lamb et al. [26–29] subtract randomly rotated and translated geometric primitives such as a cube, icosphere, and sub-divided icosphere, with and without random surface perturbation to simulate micro-scale detail. Gregor et al. [16] use spheres whose surfaces are perturbed using small-scale details of a single digitized material. In all cases, mid-scale detail is represented as cutouts via analytical primitives, which is not generalizable to real-world damage.

The Breaking Bad dataset of Sellán et al. [41] uses their earlier work [40] to model and simulate fracture modes of the object, enabling them to circumvent assumptions made by geometric methods. Their approach struggles to generate high-resolution detail, as it requires evolving the simulation over small time steps that can be computationally infeasible at a large scale. Our *Fantastic Breaks* dataset fills the gap in the lack of real-world damaged object datasets by contributing an even-now growing repository of 3D scanned real-world damaged objects rigidly aligned with 3D scans of their real-world counterparts.

Real-World Object Datasets. The capture of large-scale complete 3D scans of objects is an arduous task, due to the need for a multi-staged approach consisting of multiple presentations of the object to a scanner ensuring full coverage of hidden parts, registration of multiple scans, cleaning to correct imprecise geometry, eliminate holes, and correct deep concavities, and, depending on the application, waterproofing to ensure closed surfaces. Massive 3D datasets typically comprise single-viewpoint RGB-D images [22, 24, 47], room-scale 3D scans [11], or scans of large objects such as motorcycles, statues, benches, and tables [10] that cannot be readily impacted to capture real-world damage. The Berkeley BigBIRD dataset [42] contained 100 3D models at the time of publication and has grown to 125 models. Objects were recorded by placing on

a turntable and models were created by stitching multiple images acquired using a Kinect and Canon setup. Using the BigBIRD setup, Calli et al. [5, 6] collected the YCB dataset for a set of 77 objects as a collaboration between Yale, CMU, and UC Berkeley. Due to placement on a turntable, hidden portions, e.g., the base or concavities not visible to the cameras, are not captured. The Karlsruhe Institute of Technology (KIT) dataset [23] consists of 145 objects captured using a Konica Minolta Vi-900 digitizer, with multiple scans acquired to capture object bases.

Google Scanned Objects (GSO) [12] is perhaps the largest complete table-top 3D-scan dataset at this time, consisting of, to-date, 1,030 3D scans of household objects. GSO is collected by 3D imaging projector-cast patterns through a collaboration between robotics researchers at Google and Open Robotics since 2019. 41 researchers were involved in creating GSO. *Fantastic Breaks* has been acquired at a small rural university by 1 graduate student and 9 undergraduates, advised by 2 faculty mentors. With 156 3D scans (78 broken, 78 paired complete counterparts, and growing), *Fantastic Breaks* exceeds university tabletop datasets [5, 6, 23, 42] in total items, and is comparable to the YCB dataset in number of object identities.

Within the larger problem domain of minimizing waste, a few 2D datasets have arisen for object detection and segmentation in waste images [2, 39, 45]. Object materials span cardboard, plastic, glass, and metal. An opportunity exists to capture RGB-D images of waste, identify objects capable of being repaired, and geometrically couple them with our dataset to conduct in-the-wild repair.

Shape Repair. The creation of the *Fantastic Breaks* dataset is motivated by applications in object repair. When object parts are available, shape assembly approaches focus on joining 3D shape representations of the object parts. Geometric approaches exist to match fracture boundaries via segmentation [34, 35], feature description extraction and geometric model refinement [21], align fractured shapes to a proxy template [49], or conduct iteratively registration similar to structure from motion [19, 20]. A number of learning-based approaches exist to provide assembly, most of which assume holistic parts with simple surfaces [17, 46, 48], and one assumes arbitrary geometry at shape boundaries [9].

When parts of an object are irretrievable, shape repair approaches address generation of the lost parts. Early automation approaches to circumvent historically manual repair included finding symmetries and self-similarities in objects [16, 30, 31, 36, 43, 44], though these approaches are unsuccessful when non-symmetric object parts are broken off. One approach [25] circumvents the small-scale artifact issue of Boolean subtraction by automatically extracting and joining exterior and fractured regions for repair parts using real-world damaged and complete scans. The approach re-

quires the scan of a complete 3D proxy to be provided as input, that may not be feasible for one-of-a-kind instances, or even if available, may prove tedious to obtain.

Recent work such as 3D-ORGAN [18], MendNet [28], DeepMend [27], and DeepJoin [26] uses deep learning to conduct shape repair without knowledge of the complete proxy by representing damaged, complete, and repair shapes using voxels [18] or deep functions [26–28]. DeepMend and DeepJoin report higher success due to the use of implicit functions which enable representation to arbitrary resolutions, and due to the expression of fractured and restoration shapes in terms of constructive solid geometry operations between the complete object and a break surface whose representation is learnt during training. Though DeepMend and DeepJoin show qualitative results on a few examples of 3D scans of real-world damaged objects, in all cases, training and quantitative evaluation is conducted using datasets with synthetically-generated fractures.

3. Data Collection and Processing

Object Acquisition. We conducted a community-wide acquisition of everyday household objects that suffer damage. Our goal was to have a collection consisting not only of objects that can be damaged, but also of objects that have already suffered damage. To perform our acquisition, we made purchases at the local thrift store where we found intact and damaged objects, and requested donations from the local community. Though the *Fantastic Breaks* dataset as presented in this paper contains damaged/complete pairs, we have also collected pre-damaged objects that may lack complete counterparts, as they provide insight into real-world fracture. Our collection consists of commonly damaged household objects such as mugs, plates, and figurines spanning materials such as ceramics, plastics, glass, and wood. In some instances, we were able to pre-acquire pairs, where one object in the pair was damaged and the other was intact. In most cases, we manually damaged a complete object to obtain the broken version. When possible, we attempted to acquire pairs of complete objects, and damage one of the objects, enabling us to store physical damaged/complete pairs. We inflicted damage by dropping the object, striking the object with a rubber mallet or metal hammer, and, in 2 cases, snapping the object after anchoring it against a table. The left of Figure 2 shows an example mug with the handle shattered after striking with a mallet. Figure 3 shows example broken objects and broken/complete pairs in our dataset.

3D Scanning. We use an Einscan SP 3D turntable-based scanner to acquire 3D scans. We use Einscan’s proprietary software, EXScan, to operate the scanner. The scanning operation rotates the scanner’s turntable 8 times, acquires 8 2.5D images of the object via an attached RGB-D sensor, and fuses the images into a 3D mesh. Given the diversity of



Figure 2. Left: Complete mug on top, and broken mug on the bottom showing main intact part and the shattered handle. Right: Object on scanner with 3D scan shown in the inset.



Figure 3. Example broken objects on top and broken/complete pairs on the bottom acquired to build the *Fantastic Breaks* dataset.

object geometry where objects may contain deep concavities or complex fractures, we had to conduct careful staging of each object and perform multiple presentations of the object to maximize acquisition of the object surface. The presentation count ranged from 2 for flat objects such as plates or objects with higher convexity such as figurines, to 6 for objects with concavities such as mugs. We used the registration tool in EXScan to fuse scans into a 3D mesh.

Mesh Cleaning. Given the 3D scan of a complete or broken object, we employ a sequence of operations to ensure that the meshes are of high quality. We visually inspect each model, and if the model lacks any large holes in the mesh, we use the waterproofing tool built into EXScan to ensure that each surface is a closed 2D surface. While performing waterproofing in EXScan is preferred, if the model contains large holes or artifacts, we repair the original post-registration mesh by performing manual hole-filling using Autodesk NetFabb. For objects with deep concavities such as cups and mugs, the concavities may not have been well-presented during the scanning process, in which case the interior regions may not be metrically accurate. We repair

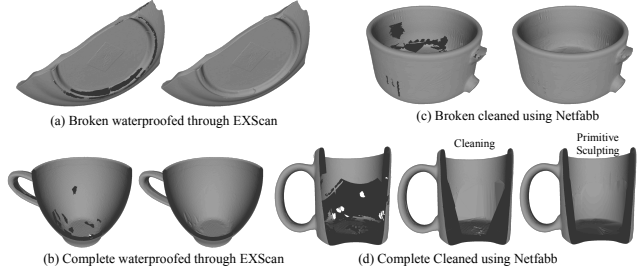


Figure 4. Meshes prior to (left) and after cleaning and waterproofing for (a) broken and (b) complete object examples waterproofed using EXScan, and (c) broken and (d) complete objects cleaned using Netfabb. For (d), we use a primitive to fix the erroneously angled surfaces created by Netfabb mesh repair tools. Complete objects are shown as cutaways to reveal pre-cleaning artifacts.

the mesh by using subtraction with a geometric primitive such as a cylinder. For a final clean, we apply the Extended Repair set of scripts in Netfabb to merge nearby vertices, remove double and flipped triangles, close all holes, wrap the mesh surface to remove interior faces, and remove small connected components. Figure 4 demonstrates examples of meshes generated using our cleaning process.

Mesh Orientation. Once each mesh is cleaned, we manually orient each mesh such that its principal axes are aligned to the Cartesian axes. We ensure that the base of the object is aligned with the xz -plane, and we rotate the object about the y -axis to ensure alignment within its category. For example, we align all mugs to ensure that the handles are aligned with the negative x direction, and all figurines so that they face in the negative x direction.

Mesh Alignment. Given the cleaned meshes for the broken object and its complete counterpart, we transform the broken mesh such that its intact regions are aligned with the corresponding regions of the complete mesh. We perform an initial manual alignment of the broken mesh to the complete mesh, and refine the alignment using the iterative closest point (ICP) [3] algorithm. We conduct a post-alignment normalization of each mesh to ensure similarly scaled data for learning-driven repair. We perform normalization by scaling the broken and complete mesh such that the complete mesh is entirely contained within a unit cube. We provide access to non-normalized and normalized meshes as part of the dataset. Figure 5 shows examples of the broken mesh aligned to the complete mesh.

Ground Truth Restoration Estimation. Our data collection involves scanning of broken objects that have either been acquired as pre-damaged, or have had damage inflicted through a destructive fracture process, such that only one part of the object remains intact. Such an occurrence is not uncommon, e.g., as shown in Figure 2, the fracture process causes the handle to further fragment into a number of small pieces that are infeasible to rescue and/or reassemble. How-

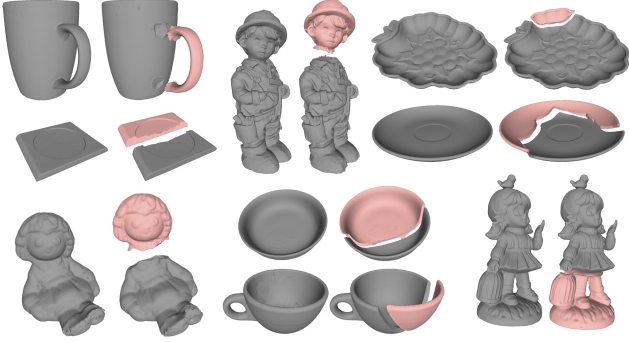


Figure 5. For each triplet of meshes, we show the complete mesh on the left, the broken mesh aligned to the complete mesh on the right, and the restoration in pink detached from the broken.

Table 1. Object distribution by class (Phys.=Physical).

	Class	Mug	Plate	Figurine	Bowl	Cup	Jar	Coaster	Box	Misc	Total
Phys.	Broken	34	28	21	14	8	7	4	3	12	131
	Complete	29	31	29	16	13	11	5	3	20	157
Scan	Broken	34	27	19	12	7	6	4	2	9	120
	Complete	29	31	28	14	8	9	5	3	18	145
	Pairs	18	21	15	8	5	5	2	1	3	78

ever, shape repair approaches can benefit from knowledge of the geometry of ground truth parts needed to complete the object shape, in order to perform training and evaluation. We contribute proxy ground truth 3D meshes for the repair parts. We synthetically generate the repair part proxies using the approach of Lamb et al. [25]. Given aligned complete and broken shapes, the approach recovers restoration meshes that smoothly join the broken shape to yield the complete geometry, lack small-scale artifacts prevalent in Boolean subtraction, and lack grooves at the fracture boundary demonstrated by approximate subtraction techniques based on a distance thresholding. Figure 5 shows restoration meshes generated for example cleaned and water-proofed 3D broken and complete scans.

Ground Truth Fracture Surface Annotation. To assist with approaches in repair that rely on accurate knowledge of the ground truth fracture surface for training or evaluation, we manually annotate triangles corresponding to the fracture surface. Figure 6 shows an example of ground truth fracture annotation.

4. Analysis of *Fantastic Breaks*

Summary of Dataset. We have annotated each object with a category level, its material, and the approach of damaging the object. At the time of this paper submission, we have acquired 131 physical damaged objects and 157 physical complete objects. Among the 131 broken objects, 14 objects are naturally damaged, and the remaining have damage inflicted manually by dropping (20) striking using

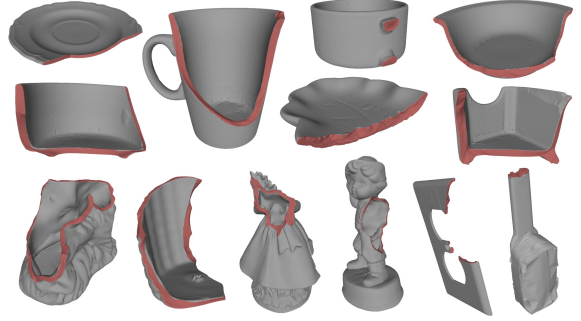


Figure 6. Broken meshes (gray) with labeled fracture surface (red).

Table 2. Object distribution by material (Mat., Phys.=Physical).

	Mat.	Ceramic	Plastic	Glass	Plaster	Wood	Other	Total
Phys.	Broken	105	14	4	3	3	2	131
	Complete	113	20	9	3	5	7	157
Scan	Broken	99	10	3	3	3	2	120
	Complete	111	17	3	3	5	6	145
	Pairs	64	7	2	3	2	0	78

a mallet (70), striking using a metal hammer (25), and anchoring and snapping (2). 108 of the broken objects have a counterpart within the 157 complete objects. We have acquired pre-cleaned scanned meshes for 120 of the broken objects and 145 of the complete objects. 78 of the 120 broken scanned objects are paired with their respective 78 complete scanned objects. These 78 pairs are fully cleaned and have restorations extracted. Tables 1 and 2 summarize physical, scanned, and paired scanned broken and complete objects by class and material respectively. It should be noted that this is a growing dataset, i.e., the physical and scanned sets are continuing to expand. We expect to have all 157 complete objects broken, and we continue to acquire, break, scan, clean, and process complete and broken objects.

Analysis of Geometric Properties. We quantitatively compare geometric properties of the *Fantastic Breaks* dataset to the *everyday* subset of *Breaking Bad* [41], and the Geometric Breaks dataset provided by Lamb et al. [26], both of which contain synthetic fractures. The *everyday* subset of *Breaking Bad* contains 542 objects each fractured 100 times, for a total of 54,200 broken objects. Breaks are obtained using a physics driven fracturing technique in which a set of fracture modes are computed and used to simulate object fracture patterns that result from an impact to the object. The Geometric Breaks dataset contains 25,449 objects from ShapeNet [7] and 1,042 objects from the GSO dataset. Objects are fractured by subtracting them with a randomized convex geometric primitive. For *Breaking Bad* we compute quantitative metrics over 78 objects selected randomly from the subset of objects in the *everyday* set that contain 2 broken parts (13,532 contain 2 broken parts).

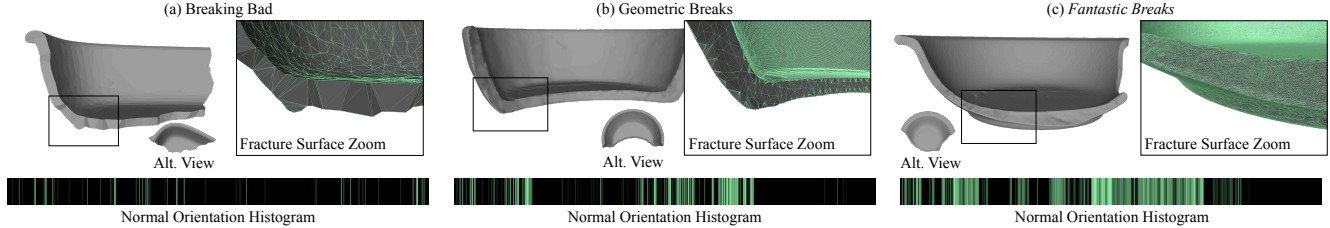


Figure 7. Broken shapes with inset showing geometric detail, alternate (alt.) top-down views, and normal orientation histograms (NOHs) for (a) Breaking Bad, (b) Geometric Breaks, and (c) *Fantastic Breaks*. NOHs are viewed as images where higher intensity lines represent higher bin counts. (a) Breaking Bad shapes show sparse structure due to limitations on fracture resolution. (b) While Geometric Breaks shapes have semi-dense structure, they demonstrate regularity attributed to the breaking primitive. (c) *Fantastic Breaks* shapes have dense surface structure and irregular break patterns characteristic of arbitrary real-world fracture.

Table 3. Number of vertices, faces, and convexity percentiles for Breaking Bad, Geometric Breaks, and *Fantastic Breaks* datasets. Max Vertices and Faces and min Convexity values are bolded.

Dataset	# Vertices	# Faces	C 25th	C 50th	C 75th
Breaking Bad	4,664.6	18,221.9	0.252	0.562	0.831
Geometric	48,624.9	97,247.7	0.568	0.751	0.910
<i>Fantastic</i>	571,869.2	1,144,518.2	0.236	0.329	0.486

For Geometric Breaks, we compute metrics over a subset of 78 randomly selected objects from the GSO and ShapeNet mugs classes. We combine the GSO and ShapeNet mugs class as the GSO dataset lacks mugs.

We provide a summary of the mean number of faces and vertices for each broken mesh in each dataset on the left of Table 3. Our broken meshes are, on average, at least ten times more dense than existing fractured object datasets. As observed by Sellán et al. [41], a common indicator of fractures generated using pre-computed fracture methods are a large number of convex fractured shapes. In the final three columns of Table 3 we provide the 25th, 50th, and 75th percentiles of broken shape convexity. We compute convexity as the ratio of the volume of the broken mesh to the volume of the mesh’s convex hull, as used by Attene et al. [1]. Highly convex shapes show a convexity value near 1. Our dataset shows a consistently lower fractured shape convexity than other datasets, with the 75th percentile of breaks showing a convexity value of 0.486, compared to 0.831 for Breaking Bad and 0.910 for Geometric Breaks.

Though synthetically generated fractured objects may show coarse geometric variation, they struggle to generate fine detail at the fractured region. As shown in Figures 7(a) and 7(b), synthetically generated fractured objects are characterized by piecewise fractured regions that lack high frequency surface variation, i.e. they do not capture the fine scale surface variability of real fractures. Simulation of object fractures with fine-scale surface variability of the same resolution as real object fractures using a

physics engine as done in Breaking Bad is intractable with current hardware. Fractures generated by subtracting geometric primitives demonstrate unnatural regularity as shown in Figure 7(b).

To quantify coarse and fine scale surface variability, we introduce the normal sparseness metric, which measures the degree to which normals on the fractured surface span the space of all possible orientations when grouped into n discrete bins. For a given broken object, we extract the fractured region of the broken mesh. We obtain n evenly spaced points on the unit sphere, and bin the normal vectors of the fractured region into one of n bins based on their closest point on the unit sphere to generate a normal orientation histogram (NOH) for the object. We show NOHs for three example objects in Figure 7. To compute the normal sparseness, we count the number of empty bins in the NOH and divide by n . A fractured region with coarse geometry is expected to show high normal sparseness as its normals are expected to span a small portion of the space of all possible orientations. The choice for n determines the scale of surface variability measured. A small value for n measures coarse surface variability, i.e. highly concave or convex fractures will have a low normal sparseness, regardless of fine scale surface geometry. A large value for n measures fine-scale surface variability. If n is large, only objects with fine-scale surface variability show low normal sparseness.

We show quantitative results for the normal sparseness for two values of n in Figure 8(a) and Figure 8(b). To measure coarse and fine surface variability, we set n to 42 and 642 respectively. As shown in Figure 8(a), *Fantastic Breaks* shows a similar sparseness spread to Geometric Breaks, indicating that both datasets contain breaks that have a high degree of coarse surface variability, though *Fantastic Breaks* contains more objects with fine surface variability, as shown the lower spread in Figure 8(b). *Fantastic Breaks* shows the lowest mean normal sparseness value of 0.253 when n is 42, compared to 0.602 for Breaking Bad and 0.359 for Geometric Breaks. As shown in Figure 8(b), *Fantastic Breaks* shows the lowest median normal sparseness

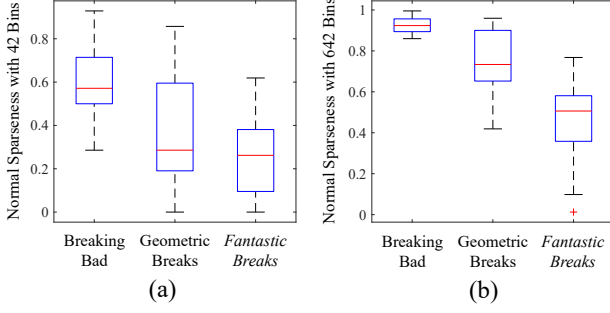


Figure 8. Box plots for distribution of normal sparseness over 78 objects from Breaking Bad, Geometric Breaks, and all objects from *Fantastic Breaks* using (a) 42 bins and (b) 642 bins.

ness when n is 642, indicating that it contains a large number of fractures with fine scale surface variability, and includes several objects with extremely low sparseness. In contrast, the piecewise fractures of Breaking Bad, and to a lesser extent Geometric Breaks, demonstrate high normal sparseness, as shown in Figure 7(a), indicating a lack of fine scale surface variability. *Fantastic Breaks* also has the lowest mean mean normal sparseness of 0.475, compared to 0.926 for Breaking Bad and 0.749 for Geometric Breaks.

5. Experimental Evaluation

As we provide complete, broken, and restoration shapes with ground truth fractured region annotations, our dataset may be used to train approaches that perform automated shape repair. We test three prior shape repair approaches on our dataset: MendNet [28], DeepMend [27], and DeepJoin [26]. These approaches generate repair parts assuming that the missing part has been lost or destroyed during the damage process. MendNet, DeepMend, and DeepJoin represent shapes by learning a function to reconstruct shapes as implicit surfaces, and require watertight 3D meshes as input. DeepJoin also requires meshes to have correct surface normals, which *Fantastic Breaks* provides.

To train shape repair methods, we pre-train a given network on a subset of the Geometric Breaks dataset or Breaking Bad dataset. For Geometric Breaks, we train with objects from the GSO and ShapeNet mugs subsets. For Breaking Bad, we train with `everyday` objects that have 2 parts. After training for 2,000 epochs on synthetically fractured objects, we train for an additional 1,000 epochs on objects from the *Fantastic Breaks* dataset. To generate training data, for each broken, complete, and restoration mesh tuple in both datasets, we sample points on the surface of each mesh and compute the signed distance function (SDF), occupancy, and normal field value for each sample point. For DeepMend and DeepJoin we compute a break surface that acts as a proxy for the fracturing process by fitting a thin-

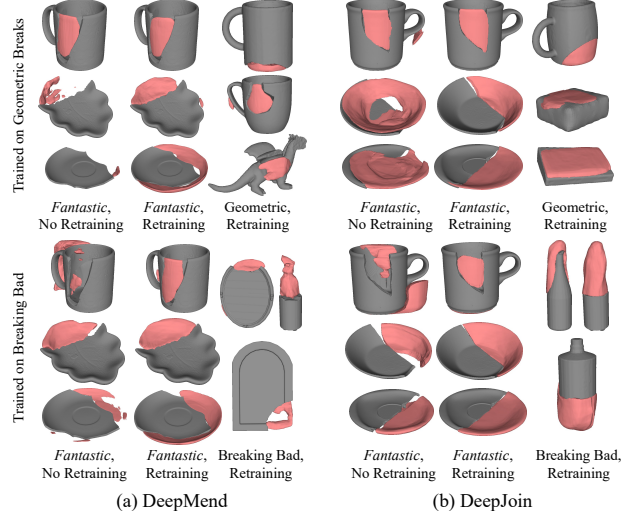


Figure 9. Predicted repair shapes in pink trained with (top) Geometric Breaks and (bottom) Breaking Bad using (a) DeepJoin and (b) DeepMend. Objects from *Fantastic Breaks* are shown before and after re-training, which improves qualitative results.

plate spline to the fractured region vertices, as described by Lamb et al. [26]. We use 812 train and 25 test objects from Geometric Breaks, and 730 train and 25 test objects from Breaking Bad. For the *Fantastic Breaks* dataset, we add objects that belong to a class with a single sample to the test set. *Fantastic Breaks* has 53 train and 25 test objects.

In Figure 9 we show repairs for broken objects before and after training on *Fantastic Breaks*. Before re-training on our real objects, DeepMend and DeepJoin may struggle to generate repairs that fully restore real objects, e.g. the plates on the left of Figure 9(a) and the plate and bowl on the left of Figure 9(b). Re-training on *Fantastic Breaks* visually improves repairs, as shown in the middle columns of Figure 9, producing more holistic repairs. As shown in the right columns of Figure 9, re-training still allows generation of repairs for synthetically fractured objects.

To measure the accuracy of predicted repairs we use the chamfer distance, as described by Park et al. [37], and normal consistency, as described by Mescheder et al. [32]. As MendNet, DeepMend, and DeepJoin perform optimization during inference to obtain repairs, inference proceeds non-deterministically. For pre-training on Geometric Breaks we report quantitative metrics over 3 re-trained models and 7 inference runs with re-training, and 21 inference runs without re-training, totaling 21 trials. For pre-training on Breaking Bad we report quantitative metrics over 1 re-trained model and 7 inference runs with re-training, and 7 inference runs without re-training, totaling 7 trials.

Table 4 shows success rate, chamfer distance and normal consistency for predicted repairs using MendNet, Deep-

Table 4. Success rate (SR), chamfer distance (CD), and normal consistency (NC), with training on Geometric Breaks (GB, top) and on Breaking Bad (BB, bottom), before (left) and after (right) re-training on *Fantastic Breaks* (FB).

	Test	Train with GB Only			Train with GB + FB		
		SR%	CD	NC	SR%	CD	NC
MendNet	GB	70.9	0.149	0.246	65.5	0.203	0.257
	FB	83.6	0.092	0.258	85.7	0.091	0.239
DeepMend	GB	99.4	0.200	0.359	96.4	0.170	0.460
	FB	93.0	0.081	0.262	99.0	0.043	0.247
DeepJoin	GB	98.5	0.159	0.395	97.7	0.153	0.529
	FB	99.0	0.031	0.270	100.0	0.025	0.259
	Test	Train with BB Only			Train with BB + FB		
		SR%	CD	NC	SR%	CD	NC
DeepMend	BB	99.4	0.103	0.385	98.9	0.172	0.254
	FB	93.7	0.050	0.451	98.9	0.041	0.500
DeepJoin	BB	99.4	0.105	0.335	100.0	0.146	0.357
	FB	100.0	0.048	0.377	100.0	0.028	0.526

Mend, and DeepJoin. As shown in the final supercolumn of Table 4 top, re-training on the *Fantastic Breaks* dataset decreases the chamfer of repair parts in all experiments except for MendNet on Geometric Breaks. As acknowledged by the authors, MendNet struggles to restore real objects when trained on synthetic fractures. Thus re-training on 53 real samples may not benefit learning. Table 4 top shows that for DeepMend and DeepJoin, re-training does not impact performance on Geometric Breaks in terms of chamfer distance and improves normal consistency. Though Table 4 bottom shows that re-training does not decrease the chamfer of Breaking Bad objects, it does increase normal consistency for DeepMend. Breaking Bad objects span a wide range of object types may have more than half of the object removed, making it a challenging dataset for repair. Re-training especially decreases the chamfer for DeepMend and DeepJoin when testing on *Fantastic Breaks* objects, from 0.081 to 0.043, and from 0.031 to 0.025 respectively when pre-trained on Geometric Breaks and from 0.085 to 0.041 and 0.048 to 0.028 when pre-trained on Breaking Bad.

6. Discussion

We present *Fantastic Breaks*, a novel dataset that contains full 360° 3D scans of broken objects geometrically aligned with 3D scans of their complete counterparts, with manual annotations of classes, materials, and fracture surfaces, and synthetic proxies for 3D meshes representing repair parts. The dataset continues to grow in number of physical objects and scans. The dataset is one of the first of its kind, enabling learning of the characteristics of fractured objects. *Fantastic Breaks* provides data-driven insight into fracture, overcoming the deficits of geometric approaches

that make prior assumptions about the damage process that are not widely applicable, as well as the concerns of datasets based on physics simulations that are limited by current hardware in modeling real-world geometry.

An obvious limitation of our endeavor is that employing destructive processes to damage objects for the purpose of real-world data acquisition is unsustainable at a large scale. We advocate that our dataset be leveraged to learn patterns of break and internal geometric structure that are common across objects of similar materials, such as ceramics or plastics, and classes, such as mugs or cups, and to use generative approaches to conduct data-driven synthesis of breaks and internal structure given 3D models of complete objects. For instance, an interesting observation of our collection is that for reasons of cost, sustainable production, and functionality, nearly all our objects have shell rather than solid structures, whereas scans of whole objects such as bottles or figurines cannot capture the internal shell structure. By exposing the internal structure, the dataset provides the opportunity to learn how to hollow out 3D models of objects, an opportunity absent from prior 3D scan datasets.

Fantastic Breaks currently contains tabletop objects that are easier to scan using desktop scanners. Larger objects may necessitate more elaborate setups, e.g., room-scale imaging systems. Future data collection can investigate the minimal number of viewpoints needed to acquire geometrically relevant understanding of internal object structure. For instance, to capture the fracture pattern of a broken chair leg, it may be sufficient to use a depth camera to image the broken region from 1-2 viewpoints, and deform the mesh of a 3D proxy of the chair acquired from a public repository to register the proxy to the viewpoints.

We have provided evaluations of existing approaches on automatic reconstruction of new repair parts using learning-driven approaches. The dataset is widely applicable to a range of other tasks, e.g., the broken and restoration meshes can be used to perform shape assembly cognizant of precision joins for real-world fracture boundaries. We evaluate shape repair approaches that do not require prior knowledge of the fractured region. However, via our manual fracture surface annotations, we also plan to release the incomplete meshes devoid of the fracture surface. These incomplete meshes will benefit research in partial shape completion [14], which up until now has largely focused on synthetically generated partial shapes or on depth scans. Datasets of real-world 3D scans have contributed to significant advancements in robotic manipulation [8, 13]. *Fantastic Breaks* provides enhanced impacts in robotics research by enabling investigation of robot-driven repair, object grasp while being cognizant of fractured regions to minimize further damage, and damaged object handling for safe human-robot handover.

References

- [1] Marco Attene, Michela Mortara, Michela Spagnuolo, and Bianca Falcidieno. Hierarchical convex approximation of 3d shapes for fast region selection. In *Computer graphics forum*, volume 27, pages 1323–1332. Wiley Online Library, 2008. 6
- [2] Dina Bashkirova, Mohamed Abdelfattah, Ziliang Zhu, James Akl, Fadi Alladkani, Ping Hu, Vitaly Ablavsky, Berk Calli, Sarah Adel Bargal, and Kate Saenko. Zerowaste dataset: Towards deformable object segmentation in cluttered scenes. In *Proceedings of the IEEE/CVF Conference on Computer Vision and Pattern Recognition*, pages 21147–21157, 2022. 3
- [3] Paul J Besl and Neil D McKay. Method for registration of 3-d shapes. In *Sensor fusion IV: control paradigms and data structures*, volume 1611, pages 586–606. Spie, 1992. 4
- [4] Benedict J Brown, Corey Toler-Franklin, Diego Nehab, Michael Burns, David Dobkin, Andreas Vlachopoulos, Christos Doumas, Szymon Rusinkiewicz, and Tim Weyrich. A system for high-volume acquisition and matching of fresco fragments: Reassembling theran wall paintings. *ACM transactions on graphics (TOG)*, 27(3):1–9, 2008. 1, 2
- [5] Berk Calli, Arjun Singh, James Bruce, Aaron Walsman, Kurt Konolige, Siddhartha Srinivasa, Pieter Abbeel, and Aaron M Dollar. Yale-cmu-berkeley dataset for robotic manipulation research. *The International Journal of Robotics Research*, 36(3):261–268, 2017. 2, 3
- [6] Berk Calli, Aaron Walsman, Arjun Singh, Siddhartha Srinivasa, Pieter Abbeel, and Aaron M Dollar. Benchmarking in manipulation research: The ycb object and model set and benchmarking protocols. *IEEE Robotics and Automation Magazine*, pages 36–52, 2015. 2, 3
- [7] Angel X Chang, Thomas Funkhouser, Leonidas Guibas, Pat Hanrahan, Qixing Huang, Zimo Li, Silvio Savarese, Manolis Savva, Shuran Song, Hao Su, et al. Shapenet: An information-rich 3d model repository. *arXiv preprint arXiv:1512.03012*, 2015. 5
- [8] Yu-Wei Chao, Wei Yang, Yu Xiang, Pavlo Molchanov, Ankur Handa, Jonathan Tremblay, Yashraj S Narang, Karl Van Wyk, Umar Iqbal, Stan Birchfield, et al. Dexycb: A benchmark for capturing hand grasping of objects. In *Proceedings of the IEEE/CVF Conference on Computer Vision and Pattern Recognition*, pages 9044–9053, 2021. 8
- [9] Yun-Chun Chen, Haoda Li, Dylan Turpin, Alec Jacobson, and Animesh Garg. Neural shape mating: Self-supervised object assembly with adversarial shape priors. In *Proceedings of the IEEE/CVF Conference on Computer Vision and Pattern Recognition*, pages 12724–12733, 2022. 1, 2, 3
- [10] Sungjoon Choi, Qian-Yi Zhou, Stephen Miller, and Vladlen Koltun. A large dataset of object scans. *arXiv preprint arXiv:1602.02481*, 2016. 2
- [11] Angela Dai, Angel X Chang, Manolis Savva, Maciej Halber, Thomas Funkhouser, and Matthias Nießner. Scannet: Richly-annotated 3d reconstructions of indoor scenes. In *Proceedings of the IEEE conference on computer vision and pattern recognition*, pages 5828–5839, 2017. 2
- [12] Laura Downs, Anthony Francis, Nate Koenig, Brandon Kinman, Ryan Hickman, Krista Reymann, Thomas B. McHugh, and Vincent Vanhoucke. Google scanned objects: A high-quality dataset of 3d scanned household items. In *2022 International Conference on Robotics and Automation (ICRA)*, pages 2553–2560, 2022. 2, 3
- [13] Hao-Shu Fang, Chenxi Wang, Minghao Gou, and Cewu Lu. Graspnet-1billion: A large-scale benchmark for general object grasping. In *Proceedings of the IEEE/CVF conference on computer vision and pattern recognition*, pages 11444–11453, 2020. 8
- [14] Ben Fei, Weidong Yang, Wenming Chen, Zhijun Li, Yikang Li, Tao Ma, Xing Hu, and Lipeng Ma. Comprehensive review of deep learning-based 3d point clouds completion processing and analysis. *arXiv preprint arXiv:2203.03311*, 2022. 8
- [15] Thomas Funkhouser, Hijung Shin, Corey Toler-Franklin, Antonio García Castañeda, Benedict Brown, David Dobkin, Szymon Rusinkiewicz, and Tim Weyrich. Learning how to match fresco fragments. *Journal on Computing and Cultural Heritage (JOCCH)*, 4(2):1–13, 2011. 1, 2
- [16] Robert Gregor, Danny Bauer, Ivan Sipiran, Panagiotis Perakis, and Tobias Schreck. Automatic 3d object fracturing for evaluation of partial retrieval and object restoration tasks-benchmark and application to 3d cultural heritage data. In *3DOR@ Eurographics*, pages 7–14, 2015. 1, 2, 3
- [17] Abhinav Narayan Harish, Rajendra Nagar, and Shanmuganathan Raman. Rgl-net: A recurrent graph learning framework for progressive part assembly. In *WACV*, pages 647–656, 2022. 1, 3
- [18] Renato Hermoza and Ivan Sipiran. 3d reconstruction of incomplete archaeological objects using a generative adversarial network. In *Proc. Computer Graphics International*, pages 5–11, 2018. 1, 3
- [19] Je Hyeong Hong, Young Min Kim, Koang-Chul Wi, and Jinwook Kim. Potsac: A robust axis estimator for axially symmetric pot fragments. In *ICCV Workshops*, pages 1421–1428, 2019. 1, 3
- [20] Je Hyeong Hong, Seong Jong Yoo, Muhammad Arshad Zee-shan, Young Min Kim, and Jinwook Kim. Structure-from-sherds: Incremental 3d reassembly of axially symmetric pots from unordered and mixed fragment collections. In *Proceedings of the IEEE/CVF International Conference on Computer Vision*, pages 5443–5451, 2021. 1, 2, 3
- [21] Qi-Xing Huang, Simon Flöry, Natasha Gelfand, Michael Hofer, and Helmut Pottmann. Reassembling fractured objects by geometric matching. In *ACM SIGGRAPH*, pages 569–578, 2006. 1, 2, 3
- [22] Allison Janoch, Sergey Karayev, Yangqing Jia, Jonathan T Barron, Mario Fritz, Kate Saenko, and Trevor Darrell. A category-level 3d object dataset: Putting the kinect to work. In *Consumer depth cameras for computer vision*, pages 141–165. Springer, 2013. 2
- [23] Alexander Kasper, Zhixing Xue, and Rüdiger Dillmann. The kit object models database: An object model database for object recognition, localization and manipulation in service robotics. *The International Journal of Robotics Research*, 31(8):927–934, 2012. 2, 3

- [24] Kevin Lai, Liefeng Bo, Xiaofeng Ren, and Dieter Fox. Rgb-d object recognition: Features, algorithms, and a large scale benchmark. In *Consumer Depth Cameras for Computer Vision*, pages 167–192. Springer, 2013. 2
- [25] N. Lamb, S. Banerjee, and N. K. Banerjee. Automated reconstruction of smoothly joining 3d printed restorations to fix broken objects. In *Proceedings of the ACM Symposium on Computational Fabrication*, pages 1–12, 2019. 1, 2, 3, 5
- [26] N. Lamb, S. Banerjee, and N. K. Banerjee. Deepjoin: Learning a joint occupancy, signed distance, and normal field function for shape repair. *ACM Trans. Graph. (Proc. SIGGRAPH Asia)*, jul 2022. 1, 2, 3, 5, 7
- [27] N. Lamb, S. Banerjee, and N. K. Banerjee. Deepmend: Learning occupancy functions to represent shape for repair. In *European Conference on Computer Vision (ECCV)*, 2022. 1, 2, 3, 7
- [28] N. Lamb, S. Banerjee, and N. K. Banerjee. Mendnet: Restoration of fractured shapes using learned occupancy functions. *Computer Graphics Forum*, 41(5):65–78, 2022. 1, 2, 3, 7
- [29] N. Lamb, N. Wiederhold, B. Lamb, S. Banerjee, and N. K. Banerjee. Using learned visual and geometric features to retrieve complete 3d proxies for broken objects. In *Symposium on Computational Fabrication*, pages 1–15, 2021. 1, 2
- [30] Xin Li, Zhao Yin, Li Wei, Shenghua Wan, Wei Yu, and Maoqing Li. Symmetry and template guided completion of damaged skulls. *Computers & Graphics*, 35(4):885–893, 2011. 1, 3
- [31] Pavlos Mavridis, Ivan Sipiran, Anthousis Andreadis, and Georgios Papaioannou. Object completion using k-sparse optimization. *Computer Graphics Forum*, 34(7):13–21, 2015. 1, 3
- [32] Lars Mescheder, Michael Oechsle, Michael Niemeyer, Sebastian Nowozin, and Andreas Geiger. Occupancy networks: Learning 3d reconstruction in function space. In *Proceedings of the IEEE/CVF conference on computer vision and pattern recognition*, pages 4460–4470, 2019. 7
- [33] Kaichun Mo, Shilin Zhu, Angel X Chang, Li Yi, Subarna Tripathi, Leonidas J Guibas, and Hao Su. Partnet: A large-scale benchmark for fine-grained and hierarchical part-level 3d object understanding. In *Proceedings of the IEEE/CVF conference on computer vision and pattern recognition*, pages 909–918, 2019. 1
- [34] Georgios Papaioannou and Evaggelia-Aggeliki Karabassi. On the automatic assemblage of arbitrary broken solid artefacts. *Image and Vision Computing*, 21(5):401–412, 2003. 1, 3
- [35] Georgios Papaioannou, E-A Karabassi, and Theoharis Theoharis. Virtual archaeologist: Assembling the past. *IEEE Computer Graphics and Applications*, 21(2):53–59, 2001. 1, 3
- [36] Georgios Papaioannou, Tobias Schreck, Anthousis Andreadis, Pavlos Mavridis, Robert Gregor, Ivan Sipiran, and Konstantinos Vardis. From reassembly to object completion: A complete systems pipeline. *Journal on Computing and Cultural Heritage*, 10(2):1–22, 2017. 1, 3
- [37] Jeong Joon Park, Peter Florence, Julian Straub, Richard Newcombe, and Steven Lovegrove. DeepSDF: Learning continuous signed distance functions for shape representation. In *Proc. CVPR*, pages 165–174, Piscataway, NJ, 2019. IEEE. 7
- [38] Angelia Payne, Keenan Cole, Katie Simon, Christopher Goodmaster, and Fredrick Limp. Designing the next generation virtual museum: Making 3d artifacts available for viewing and download. In *Making History Interactive: Proceedings of the 37th Annual International Conference on Computer Applications and Quantitative Methods in Archaeology (CAA)*, volume 3, pages 1–6, 2009. 2
- [39] Pedro F Proença and Pedro Simões. Taco: Trash annotations in context for litter detection. *arXiv preprint arXiv:2003.06975*, 2020. 3
- [40] Silvia Sellán, Jack Luong, Leticia Mattos Da Silva, Aravind Ramakrishnan, Yuchuan Yang, and Alec Jacobson. Breaking good: Fracture modes for realtime destruction. *ACM Trans. Graph.*, jul 2022. 1, 2
- [41] S. Sellán et al. Breaking bad. In *NeurIPS*, 2022. 1, 2, 5, 6
- [42] Arjun Singh, James Sha, Karthik S Narayan, Tudor Achim, and Pieter Abbeel. Bigbird: A large-scale 3d database of object instances. In *2014 IEEE international conference on robotics and automation (ICRA)*, pages 509–516. IEEE, 2014. 2, 3
- [43] Ivan Sipiran. Completion of cultural heritage objects with rotational symmetry. In *Proceedings of the 11th Eurographics Workshop on 3D Object Retrieval*, pages 87–93, 2018. 1, 3
- [44] Ivan Sipiran, Robert Gregor, and Tobias Schreck. Approximate symmetry detection in partial 3d meshes. *Computer Graphics Forum*, 33(7):131–140, 2014. 1, 3
- [45] Joao Sousa, Ana Rebelo, and Jaime S Cardoso. Automation of waste sorting with deep learning. In *2019 XV Workshop de Visão Computacional (WVC)*, pages 43–48. IEEE, 2019. 3
- [46] Rundui Wu, Yixin Zhuang, Kai Xu, Hao Zhang, and Baoquan Chen. Pq-net: A generative part seq2seq network for 3d shapes. In *Proceedings of the IEEE/CVF Conference on Computer Vision and Pattern Recognition*, pages 829–838, 2020. 1, 3
- [47] Yu Xiang, Wonhui Kim, Wei Chen, Jingwei Ji, Christopher Choy, Hao Su, Roozbeh Mottaghi, Leonidas Guibas, and Silvio Savarese. Objectnet3d: A large scale database for 3d object recognition. In *European conference on computer vision*, pages 160–176. Springer, 2016. 2
- [48] Guanqi Zhan, Qingnan Fan, Kaichun Mo, Lin Shao, Baoquan Chen, Leonidas J Guibas, Hao Dong, et al. Generative 3d part assembly via dynamic graph learning. *Advances in Neural Information Processing Systems*, 33:6315–6326, 2020. 1, 3
- [49] Kang Zhang, Wuyi Yu, Mary Manhein, Warren Waggenspack, and Xin Li. 3d fragment reassembly using integrated template guidance and fracture-region matching. In *Proceedings of the IEEE international conference on computer vision*, pages 2138–2146, 2015. 1, 3

- [50] Qingnan Zhou and Alec Jacobson. Thingi10k: A dataset of 10,000 3d-printing models. *arXiv preprint arXiv:1605.04797*, 2016. [1](#)